Journal of Engineering and Technology for Industrial Applications

ITEGAM-JETIA

ISSN ONLINE: 2447-0228

Manaus, v.11 n.51, p. 56-64. January/February., 2025.
DOI: https://doi.org/10.5935/jetia.v11i51.1411

RESEARCH ARTICLE　　OPEN ACCESS

THE INFLUENCE OF THE GEOMETRIC FEATURES OF PROCESSED SURFACES ON CONTACT INTERACTION AND PROCESS PERFORMANCE DURING MACHINING WITH ELASTIC POLYMER-ABRASIVE WHEELS

Dmitriy Podashev

Kaliningrad State Technical University – Kaliningrad, Russia.

[1]http://orcid.org/0000-0001-9112-9253

Email: dmitrij.podashev@klgtu.ru

ARTICLE INFO

Article History
Received: November 18, 2024
Revised: December 20, 2024
Accepted: January 15, 2025
Published: January 30, 2025

Keywords:
flexible polymer-abrasive wheel,
machining process efficiency,
processing modes,
contact length,
surface geometry.

ABSTRACT

The automation of finishing and deburring operations remains a highly relevant task for modern mechanical engineering. This article examines the study of the influence of the specifics of contact interaction between various polymer-abrasive wheels on the productivity of the machining process in order to determine the relationship between the geometric shape of the processed surface and the productivity of the processing process. For theoretical calculations and experimental studies, elastic polymer-abrasive discs from 3M, models FS-WL, DB-WL, and CF-FB were used. The experimental research was conducted using a modern robotic complex based on the KUKA KR 210 R2700 EXTRA industrial robot. Interaction schemes of wheels with different surfaces are considered, and formulas are determined for each of them that allow calculating the average deformation and the length of the contact area. The effect of the average deformation and length of the contact zone on the efficiency of the treatment process is proven. These results should be taken into account when optimizing the operations under consideration, as well as when designing technological processes for finishing parts using elastic polymer-abrasive tools.

I. INTRODUCTION

At present, the role of transport in the Russian economy is very significant. This is due to the volume of passenger, cargo, and baggage transportation in Russia, the longest country on Earth. Transport is a crucial element in ensuring the welfare of both the state and its population, making the development of a medium-haul narrow-body aircraft an important direction for the transport engineering industry in the Russian Federation.

The MC-21 aircraft (Figure 1) belongs to the family of modern Russian mainline airliners developed by the Yakovlev Corporation under the framework of the Russian Federal Government program “Development of the Aviation Industry for the period 2013-2025.”

The MC-21-300 aircraft modification has a seating capacity ranging from 163 to 211 passengers. It is designed for the most popular segment of the passenger transportation market in the Russian Federation and boasts the largest cabin width and aisle width in its class. The MC-21 fully meets high international standards and industry requirements in terms of safety.

Flight performance characteristics	
Aircraft length, m	42,3
Wingspan, m	35,9
Aircraft height, m	11,5
Cabin width, m	3,81
Fuselage width, m	4,06
Maximum takeoff weight, kg	79 250
Maximum landing weight, kg	69 100
Maximum commercial load, kg	22 600
Maximum fuel capacity, kg	20 400
Maximum range in two-class configuration, km	5 900

Figure 1: General appearance and flight performance characteristics of the MC-21-300 aircraft.
Source: Authors, (2025).

An analysis of the nomenclature of fuselage parts of this aircraft showed that it contains more than 500 different parts made of aluminum and titanium alloys, on which finishing and polishing operations are carried out.

Currently, the share of manual labor involved in performing these operations remains significant, negatively affecting labor productivity and, consequently, the cost of the final product.

Almost all structural parts of the aircraft made of aluminum alloys require smoothing to reduce roughness to required values. The need for this operation often arises at transition points, when changing the feed direction, or when processing curved surfaces because the required surface roughness specified in the drawings is not achieved. It should be noted that the dimensions of these parts reach 500...2000 mm or more, and it is advisable to perform their processing in a fixed and oriented position. Examples include stringers, rims, sections of skin between frames, hull skin sections, profiles, etc. (Figure 2).

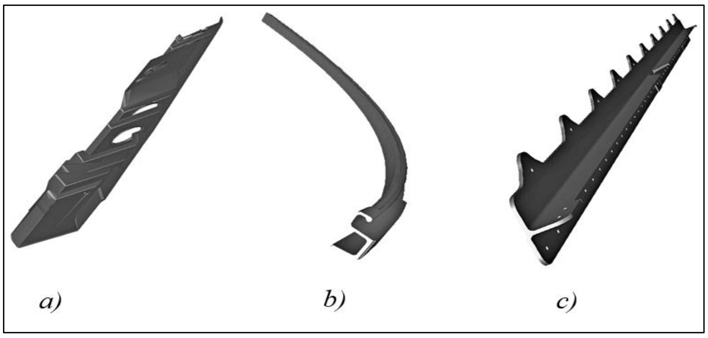

Figure 2: Examples of complex-profile, large-sized aircraft frame parts: a) stringer; b) rim; c) profile.
Source: Authors, (2025).

It should be noted that when using rigid tools, it is difficult to smooth a thin surface layer to reduce roughness (especially for parts made of aluminum alloys, widely used in aerospace construction) due to the possibility of removing a certain amount of material and compromising the required dimensional accuracy.

Methods of bulk vibration and magnetic-abrasive processing, as well as other well-known methods, are very effective and actively applied for the finish processing of metal parts with overall dimensions up to 300 mm [1-3]. However, applying these methods to large-scale and long-length parts shown in Figure 2 is economically impractical since they require bulky and expensive equipment, as well as extensive preparatory and concluding work.

Based on the above, it can be concluded that the most promising approach capable of effectively addressing these issues related to ensuring the quality of finish processing for large-scale, complex-profiled, and long-length parts considering their size and design features, is processing with polymer-abrasive wheels bonded with non-woven materials and brushes (radial and end-face), which possess high flexibility. A similar situation is observed in other areas of mechanical engineering production.

Thus, there exists a serious technological challenge associated with the necessity to automate finishing and deburring operations in serial production environments.

Numerous works [4-13] have been dedicated to the topics of contact interaction, process efficiency, formation of the surface layer, and the quality of the processed surface in various types of mechanical processing. Currently, attempts have been made to automate these technological operations using cutting tools [14], [15] and flap discs [16],[17]. However, these well-known technologies and recommendations are difficult to apply when processing parts made from aluminum alloys where it is necessary to smooth a thin surface layer. This is especially true for shaped surfaces, where the use of absolutely rigid tools or flexible tools with relatively high rigidity (such as flap discs) leads to a high percentage of defects and significant economic losses for the production.

II. MATERIALS AND METHODS

One of the most promising directions capable of efficiently addressing these problems is processing with polymer-abrasive wheels with nonwoven bonding and solid-bristle brushes (both radial and end-facing), which exhibit high flexibility. At present, the processing with such tools is insufficiently studied, and corresponding theoretical and experimental investigations to determine process efficiency indicators and the quality of processed surfaces in relation to the specifics of contact interactions between these tools and various surfaces and geometrical features of the parts being processed are lacking. To make a scientifically sound choice of flexible polymer-abrasive tools and processing regimes, knowledge about their influence on process efficiency and the quality of the surface layer taking into account the geometrical peculiarities of the surfaces being processed is essential.

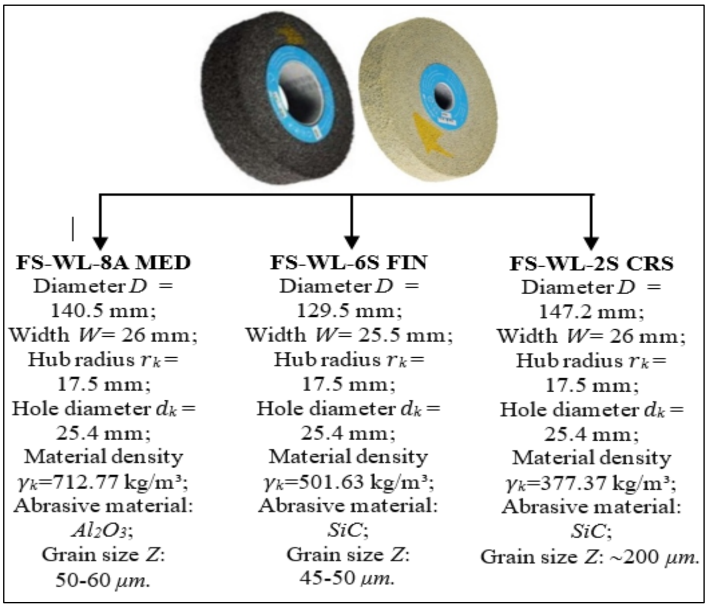

Figure 3: Molded wheels brand FS-WL.
Source: Authors, (2025).

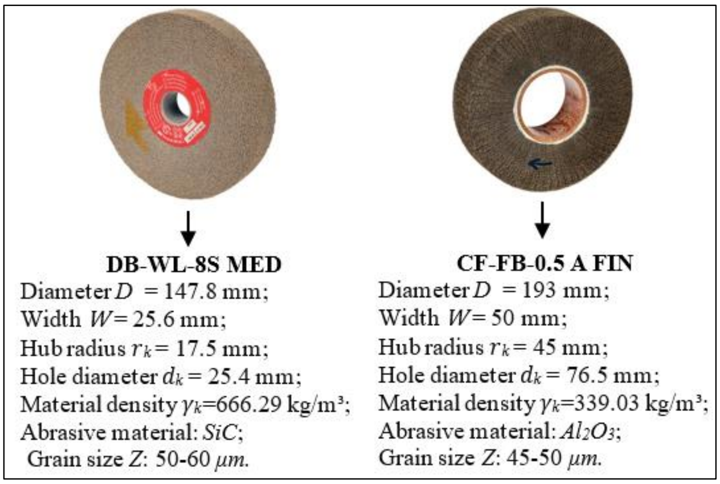

Figure 4: Molded wheel brand DB-WL and flexible wheel consisting of lamellae brand CF-FB.
Source: Authors, (2025).

The experimental part of this work was carried out using elastic polymer-abrasive wheels from the company 3M, shown in Figures 3-4. These wheels are made of non-woven abrasive material Scotch-Brite™.

III. RESULTS AND DISCUSSIONS

Features of contact interaction between elastic polymer-abrasive tools and processed surfaces

Analysis of the designs of MC-21 aircraft frame parts allowed us to identify three variants that determine the features of tool-part contact interaction: contact with a flat surface, as well as contact with surfaces rounded along an external radius and internal radius. For a given circle deformation ΔY in all cases of circle contact with different surfaces (flat, rounded along the outer radius, rounded along the inner radius), the angle α (Figures 5, 6, 7) will be determined as:

$$\cos\alpha = 1 - \frac{\Delta Y}{R}$$

In the case of contact interaction between an elastic polymer-abrasive wheel and a flat surface: $\Delta Y = \Delta Y_w$.

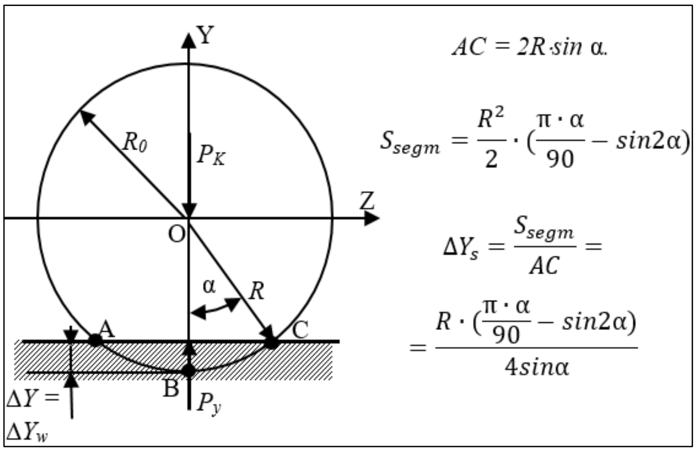

Figure 5: Interaction scheme with a flat surface.
Source: Authors, (2025).

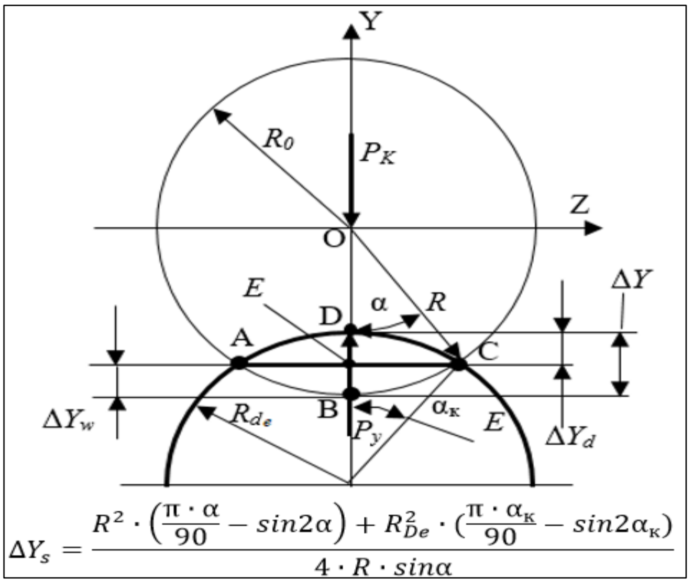

Figure 6: Interaction scheme with a surface rounded along the outer radius.
Source: Authors, (2025).

In Figure 5: S_{segm} is the area of segment ABC; ΔY_w is the average weighted deformation of the circle. The angle α here is in degrees.

For the case of contact between the circle and the surface rounded along the outer radius (Figure 6):

$$\Delta Y = \Delta Y_w + \Delta Y_d$$

For the case of contact between the circle and the surface rounded along the inner radius (Figure 7):

$$\Delta Y = \Delta Y_w - \Delta Y_d$$

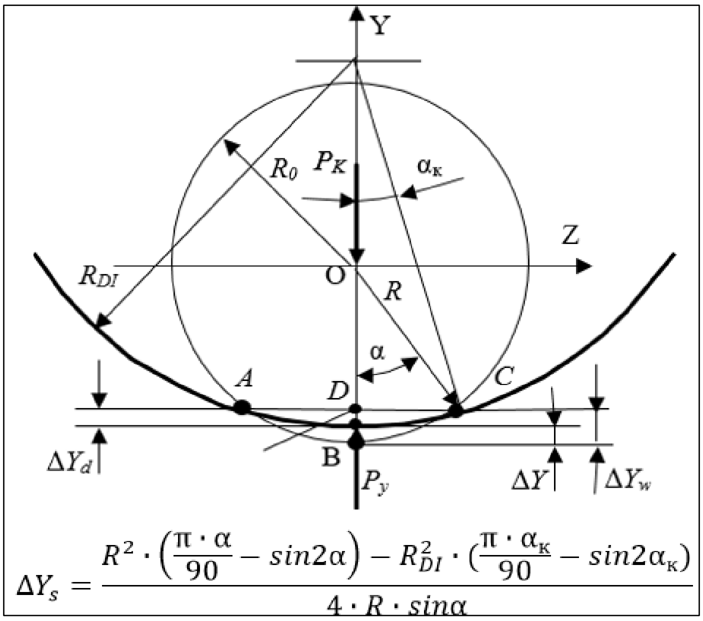

Figure 7: Interaction scheme with a surface rounded along the inner radius.
Source: Authors, (2025).

The length of the contact zone between the wheel and the workpiece surface

The length of the contact zone between the wheel and the workpiece surface depends on the specified wheel deformation ΔY and the geometric shape of the workpiece surface.

For the case of contact between the wheel and a flat surface *(see Figure 5)*, the length of the contact zone for a given wheel deformation ΔY is calculated using the formula:

$$L_c = 2\sqrt{\Delta Y \cdot R - \Delta Y^2} \quad (1)$$

For the case of contact between the wheel and the surface rounded along the outer radius *(see Figure 6):*

$$L_c = \alpha_k \cdot R_{de} \quad (2)$$

where α_κ is the contact angle between the part and the wheel in radians, defined by the condition that $\Delta Y = \Delta Y_w + \Delta Y_d$, since $\Delta Y_w \cdot R = \Delta Y_d \cdot R_{de}$, and $\Delta Y_d = R_{de} \cdot (1 - \cos \alpha_\kappa/2)$.

After transformation:

$$\cos\frac{\alpha_K}{2} = 1 - \Delta Y \cdot \frac{R}{(R_{de}+R) \cdot R_{de}},$$

where R – is the radius of the elastic polymer-abrasive wheel, mm; R_{de} – is the rounding radius of the workpiece surface, mm.

For the case of contact between the wheel and the surface rounded along the inner radius (see Figure 7):

$$L_c = \alpha_k \cdot R_{DI} \,, \tag{3}$$

where $cos\frac{\alpha_к}{2} = 1 - \Delta Y \cdot \frac{R}{(R_{DI}-R)\cdot R_{DI}}$.

Determination of the processing performance using elastic polymer-abrasive wheels in relation to the geometrical characteristics of the machined surfaces

Material removal during the studied processing method occurs through the interaction of abrasive grains from the elastic polymer-abrasive wheel with the workpiece surface. It includes both the volume of material displaced in the form of chips and the material destroyed due to repeated plastic and elastic deformation (poly-deformation), which results from numerous overlapping impacts of the abrasive particles.

It is known that the volume of elastically and plastically deformed material is negligible compared to the volumes of chips.

Therefore, the formula for material removal per unit area per unit time can be written as follows:

$$Q = W \cdot l_{ws} \cdot Q_v \cdot T \cdot n, \tag{4}$$

where: W – width of processing, mm; l_{ws} – length of the workpiece surface, mm; n – rotational speed of the wheel, rpm; T – processing time for length l_{ws}, min.:

$$T = \frac{l_{ws}}{F_R} \,, \tag{5}$$

where F_R – longitudinal feed rate, mm/min; Q_v – volume of material removed by the elastic polymer-abrasive wheel per single revolution per unit width (1 mm) when moving into contact with the workpiece over a distance of 1 mm.

$$Q_v = C_S \cdot N_g \cdot 2\pi \cdot R \cdot L_c \,, \tag{6}$$

where: C_S – cross-sectional area of the chip on a single grain; N_g – number of grains of the elastic polymer-abrasive wheel in contact on an area of 1 mm²; L_c– length of the contact zone at a given wheel deformation ΔY, which depends on the geometric shape of the workpiece surface (see equations (1-3)); R – radius of the wheel, mm.

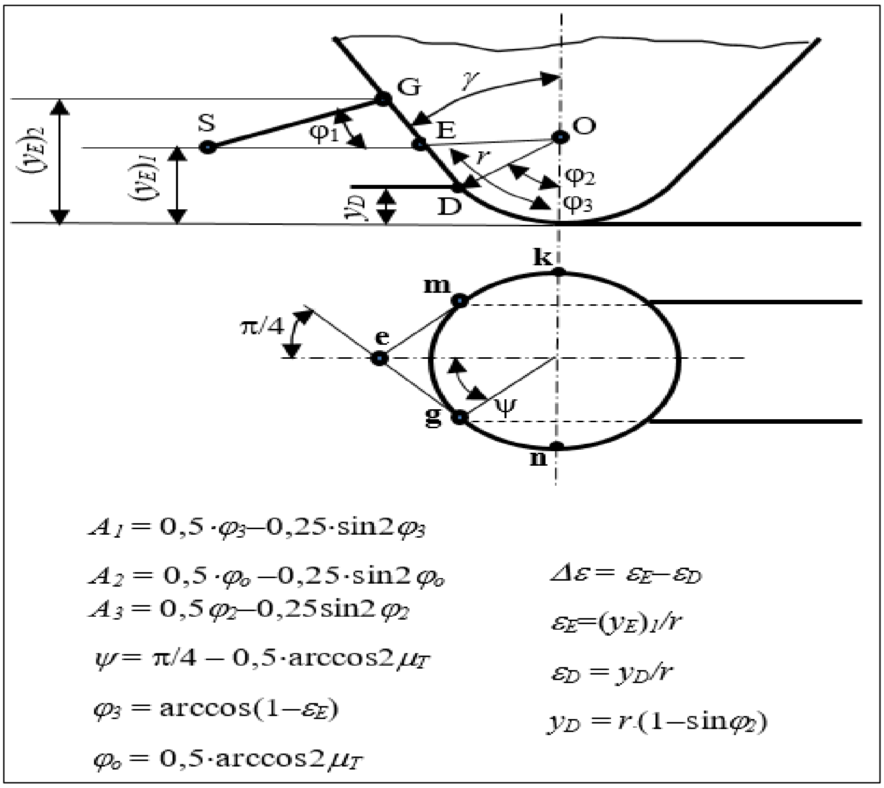

Figure 8: Interaction of a single-grain model with the workpiece surface.
Source: Authors, (2025).

The cross-sectional area of the chip on a single grain (Cs) and the number of grains of the elastic polymer-abrasive wheel in contact on an area of 1 mm² (Ng), which need to be determined for calculating the material removal per unit area per unit time, are calculated taking into account the specific physical and mechanical properties of the thin near-surface layer of the material, and the determination of micro-relief parameters of real elastic polymer-abrasive wheels according to a specially developed methodology [18]. When a grain penetrates the surface at an angle, a bulge forms ahead of it (Figure 8), which under certain conditions may turn into a chip. Plastically pushed aside material flows around the grain without separating from the main mass, forming a buildup on its sides.

In Figure 8, the following notations are used: $(y_E)_1$ – depth of penetration of the elastic polymer-abrasive wheel grain; mg – section where chip formation occurs; D – point where the spherical part transitions into the conical part; mk and gn – sections where, upon movement of the grain, the material is plastically pushed aside to form a build-up. Angles φ_2, φ_3 and φ_o are in radians.

Cross-sectional area of the chip on a single grain:

$$C_S = 2r^2 \cdot \sin\psi \cdot (A_1 - A_2), \text{ when } (y_E)_1 \le y_D; \tag{7}$$

$$C_S = 2r^2 \cdot \sin\psi \cdot [A_3 + A_2 + \Delta\varepsilon \cdot (0{,}5 \cdot \Delta\varepsilon \cdot ctg\varphi_2 + \sin\varphi_2)], \tag{8}$$

when $(y_E)_1 > y_D$,

where r is the radius of curvature of the abrasive grain throughout the entire cutting microrelief, and ψ is the angle of the stalled section on a spherical abrasive grain.
After transformations, we obtain:

$$C_S = 0{,}864 \cdot r^2 \cdot [0{,}5\varphi_3 + 0{,}25 sin2\varphi_3 - 0{,}5617], \qquad (9)$$

when $(y_E)_1 \leq y_D$;

$$C_S = 0{,}864 \cdot r^2 \cdot \left[0{,}5\left(\frac{(y_E)_1}{r}\right)^2 + 0{,}414\left(\frac{(y_E)_1}{r}\right) - 0{,}1642\right], \qquad (10)$$

when $(y_E)_1 > y_D$,

Here $(y_E)_1$– the expected value of the penetration depth of plastically deforming material protrusions of grains.

To determine $(y_E)_1$, the dependencies of the cutting force components for a single grain are used. These issues are discussed in more detail in works [19], [20]. It should be noted that when dealing with small depths of penetration of the cutting microrelief during processing with elastic polymer-abrasive wheels, it is virtually impossible to take into account all factors related to the constantly changing microgeometry due to tool wear and self-sharpening. In light of this, for elastic polymer-abrasive wheels, the decision was made to experimentally determine the actual radius r_1 based on the level of convergence γ_k, and consequently, on the processing parameters — ΔY, V, and F_R. The experimentally obtained dependence of the radius of curvature of the grain vertices on the treatment modes (ΔY, V and F_R) takes the form:

$$r_1 = a_1 \cdot \Delta Y^2 + a_2 \cdot V^2 + a_3 \cdot F_R{}^2 + a_4 \cdot \Delta Y + a_5 \cdot V + a_6 \cdot F_R + a_7 \cdot \Delta Y \cdot V + a_8 \cdot \Delta Y \cdot F_R + a_9 \cdot V \cdot F_R + a_{10} \cdot \Delta Y \cdot V \cdot F_R + a_{11}. \qquad (11)$$

The values of the coefficients a_1 through a_{10} and the free term a_{11} for equation (11) are given in Table 1. The cutting speeds V are in m/s, wheel deformation ΔY is in mm, and feed rate F_R is in m/min.

Thus, in equations (9) and (10), one should assume: $r = r_1$.
To confirm the adequacy of the developed theoretical propositions, corresponding experimental studies were conducted. In these experiments, elastic polymer-abrasive wheels from 3M, shown in Figures 3–4, were used.

The results of calculating the processing productivity Q according to formula (4), as well as the contact length L_c according to formulas (1-3) for various wheels, are presented in Tables 2-6. As an example, cases of wheel contact with a flat surface, a surface rounded by the outer radius R_{de}=120 mm, and a surface rounded by the inner radius R_{DI}=120 mm are considered.

Table 1: Values of coefficients and free term in formula (11).

Coefficient	Wheels brand FS-WL 8A MED	Wheels brand FS-WL 6S FIN	Wheels brand FS-WL 2S CRS	Wheel brand DB-WL 8S MED	Wheel brand CF-FB 0,5A FIN
a_1	$6{,}01 \cdot 10^{-4}$	$5{,}503 \cdot 10^{-3}$	$6{,}448 \cdot 10^{-4}$	$4{,}99 \cdot 10^{-5}$	$3{,}599 \cdot 10^{-5}$
a_2	–	$5{,}56 \cdot 10^{-9}$	$1{,}389 \cdot 10^{-9}$	–	–
a_3	$-1{,}39 \cdot 10^{-8}$	$-1{,}1 \cdot 10^{-9}$	–	$-1{,}01 \cdot 10^{-8}$	$-2{,}5 \cdot 10^{-9}$
a_4	$4{,}002 \cdot 10^{-3}$	$-0{,}01445$	$1{,}488 \cdot 10^{-4}$	$3{,}99 \cdot 10^{-3}$	$9{,}005 \cdot 10^{-5}$
a_5	–	$8{,}331 \cdot 10^{-7}$	$8{,}333 \cdot 10^{-7}$	$3{,}332 \cdot 10^{-7}$	$1{,}667 \cdot 10^{-8}$
a_6	$-1{,}51 \cdot 10^{-6}$	$-4{,}98 \cdot 10^{-8}$	–	$-1{,}01 \cdot 10^{-6}$	$-4{,}99 \cdot 10^{-8}$
a_7	–	$1{,}167 \cdot 10^{-9}$	$1{,}167 \cdot 10^{-9}$	–	–
a_8	$4{,}995 \cdot 10^{-7}$	$-5{,}01 \cdot 10^{-6}$	–	$4{,}99 \cdot 10^{-7}$	$2{,}501 \cdot 10^{-8}$
a_9	–	$6{,}665 \cdot 10^{-9}$	–	–	–
a_{10}	–	$1{,}66 \cdot 10^{-11}$	–	–	–
a_{11}	$1{,}404 \cdot 10^{-3}$	$0{,}0147$	$2{,}01 \cdot 10^{-4}$	$-1{,}29 \cdot 10^{-3}$	$3{,}004 \cdot 10^{-5}$

Source: Authors, (2025).

Table 2: Results of calculating contact length L_c and process productivity Q when processing surfaces with an elastic polymer-abrasive wheel FS-WL 8A MED.

V, m/min	F_R, mm/min	ΔY, mm	Flat surface: L_c, mm (1)	Flat surface: Q, μm/min (4)	Surface rounded along the outer radius R_{de}=120 mm: L_c, mm (2)	Surface rounded along the outer radius R_{de}=120 mm: Q, μm/min (4)
220,7	130	1,5	28,88	52,94	23,068	50,881
441,4				87,35		80,147
551,7				101,11		92,569
706,2				101,44		97,668
441,4	130	0,5	16,733	25,89	13,315	23,14
		1,0	23,622	58,14	18,832	55,98
		1,5	28,88	87,35	23,068	80,147
		2,0	33,287	120,1	26,64	101,86
441,4	42	1,5	28,88	27,39	23,068	19,45
	130			87,35		80,147
	255			207,82		174,12
	395			278,17		223,57

V, m/min	F_R, mm/min	ΔY, mm	Surface rounded along the inner radius R_{DI}=120 mm: L_c, mm (3)	Surface rounded along the inner radius R_{DI}=120 mm: Q, μm/min (4)
220,7	130	1,5	45,159	62,4
441,4				134,76
551,7				158,11
706,2				169,62
441,4	130	0,5	26,047	34,19
		1,0	36,854	65,56
		1,5	45,159	134,76
		2,0	52,171	171,12
441,4	42	1,5	45,159	40,12
	130			134,76
	255			256,55
	395			377,12

Source: Authors, (2025).

Table 3: Results of calculating contact length L_c and process productivity Q when processing surfaces with an elastic polymer-abrasive wheel FS-WL 6S FIN.

V, m/min	F_R, mm/min	ΔY, mm	Flat surface: L_c, mm (1)	Flat surface: Q, μm/min (4)	Surface rounded along the outer radius R_{de}=120 mm: L_c, mm (2)	Surface rounded along the outer radius R_{de}=120 mm: Q, μm/min (4)
203,4	130	1,5	27,713	5,075	22,473	4,975
406,8				7,446		7,120
508,5				8,45		8,147
650,9				8,665		8,415
406,8	130	0,5	16,062	1,456	12,972	1,411
		1,0	22,672	3,62	18,347	3,15
		1,5	27,713	7,446	22,473	7,120
		2,0	31,937	10,443	25,953	9,812
406,8	42	1,5	27,713	3,937	22,473	3,737
	130			7,446		7,120
	255			11,889		10,802
	395			16,105		15,455

V, m/min	F_R, mm/min	ΔY, mm	Surface rounded along the inner radius R_{DI}=120 mm: L_c, mm (3)	Surface rounded along the inner radius R_{DI}=120 mm: Q, μm/min (4)
203,4	130	1,5	41,131	6,274
406,8				10,567
508,5				12,642
650,9				13,046
406,8	130	0,5	23,727	1,921
		1,0	33,569	4,971
		1,5	41,131	10,567
		2,0	47,513	16,264
406,8	42	1,5	41,131	5,012
	130			10,567
	255			17,802
	395			25,456

Source: Authors, (2025).

Table 4: Results of calculating contact length L_c and process productivity Q when processing surfaces with an elastic polymer-abrasive wheel FS-WL 2S CRS.

V, m/min	F_R, mm/min	ΔY, mm	Flat surface		Surface rounded along the outer radius R_{de}=120 mm	
			L_c, mm (1)	Q, µm/min (4)	L_c, mm (2)	Q, µm/min (4)
231,2	130	2,5	38,039	25,856	30,226	22,801
464,4				44,962		40,116
578,1				55,569		49,802
739,9				61,475		57,027
464,4	130	1,5	29,567	8,980	23,407	8,205
		2,0	34,082	21,746	27,031	19,106
		2,5	38,039	44,962	30,226	40,116
		3,0	41,598	77,591	33,115	69,997
464,4	42	2,5	38,039	39,006	30,226	37,201
	130			44,962		40,116
	255			54,522		50,964
	395			66,749		59,427

V, m/min	F_R, mm/min	ΔY, mm	Surface rounded along the inner radius R_{DI}=120 mm	
			L_c, mm (3)	Q, µm/min (4)
231,2	130	2,5	61,871	34,124
464,4				55,455
578,1				70,229
739,9				84,023
464,4	130	1,5	47,872	12,101
		2,0	55,309	29,789
		2,5	61,871	55,455
		3,0	67,814	97,199
464,4	42	2,5	61,871	46,102
	130			55,455
	255			64,106
	395			75,991

Source: Authors, (2025).

Table 5: Results of calculating contact length L_k and process productivity Q when processing surfaces with an elastic polymer-abrasive wheel DB-WL 8S MED.

V, m/min	S, mm/min	ΔY, mm	Flat surface		Surface rounded along the outer radius R_{de}=120 mm	
			L_k, mm (1)	Q, µm/min (4)	L_k, mm (2)	Q, µm/min (4)
232,2	130	1,5	29,628	61,010	23,436	56,809
464,3				103,11		94,996
580,4				123,98		111,28
742,9				126,97		118,21
464,4	130	0,5	17,164	38,225	13,527	32,882
		1,0	24,232	44,623	19,133	41,113
		1,5	29,628	103,11	23,436	94,996
		2,0	34,153	136,4	27,065	121,78
464,4	42	1,5	29,628	31,5	23,436	29,105
	130			103,11		94,996
	255			199,03		182,22
	395			299,93		256,11

V, m/min	S, mm/min	ΔY, mm	Surface rounded along the inner radius R_{DI}=120 mm	
			L_k, mm (3)	Q, µm/min (4)
232,2	130	1,5	48,126	70,104
464,3				135,99
580,4				154,41
742,9				176,19
464,4	130	0,5	27,755	50,447
		1,0	39,273	66,601
		1,5	48,126	135,99
		2,0	55,602	178,64
464,4	42	1,5	48,126	40,221
	130			135,99
	255			246,97
	395			386,02

Source: Authors, (2025).

Table 6: Results of calculating contact length L_k and process productivity Q when processing surfaces with an elastic polymer-abrasive wheel CF-FB-0,5AFIN.

V, m/min	F_R, mm/min	ΔY, mm	Flat surface		Surface rounded along the outer radius R_{de}=120 mm	
			L_c, mm (1)	Q, µm/min (4)	L_c, mm (2)	Q, µm/min (4)
303,2	130	4	54,991	25,858	41,423	17,155
606,3				40,183		29,881
757,9				45,221		34,789
970,1				45,906		39,102
606,3	130	3	47,749	32,534	35,862	21,199
		3,5	51,507	36,317	38,741	25,556
		4,0	54,991	40,183	41,423	29,881
		4,5	58,249	44,294	43,942	33,994
606,3	42	4	54,991	6,131	41,423	5,012
	130			40,183		29,881
	255			87,601		67,105
	395			134,17		102,29

V, m/min	F_R, mm/min	ΔY, mm	Surface rounded along the inner radius R_{DI}=120 mm	
			L_c, mm (3)	Q, µm/min (4)
303,2	130	4	127,05	38,111
606,3				65,256
757,9				76,101
970,1				82,604
606,3	130	3	109,7	39,186
		3,5	118,67	52,349
		4,0	127,05	65,256
		4,5	134,96	78,777
606,3	42	4	127,05	9,115
	130			65,256
	255			141,5
	395			206,98

Source: Authors, (2025).

Figure 9: Robotic complex based on KUKA KR 210 R2700 EXTRA industrial robot.
Source: Authors, (2025).

Experimental studies were carried out using a robotic complex based on the KUKA KR 210 R2700 EXTRA industrial robot (Figure 9). The process productivity was evaluated by weighing the samples before and after processing using Ohaus Discovery series analytical scales, model DV214C. The workpiece material used was the alloy V95pchT2, which is a typical representative of high-strength aluminum alloys widely used in aerospace engineering.

The processing schemes for surfaces rounded along the outer and inner radii are shown in Figures 10 and 11.

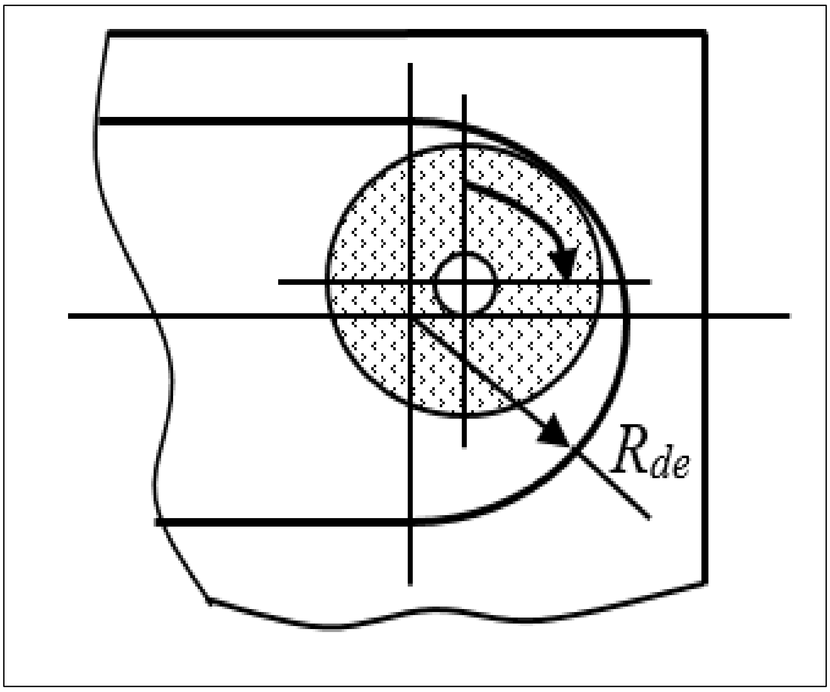

Figure 10: Scheme for processing a surface rounded along the inner radius.
Source: Authors, (2025).

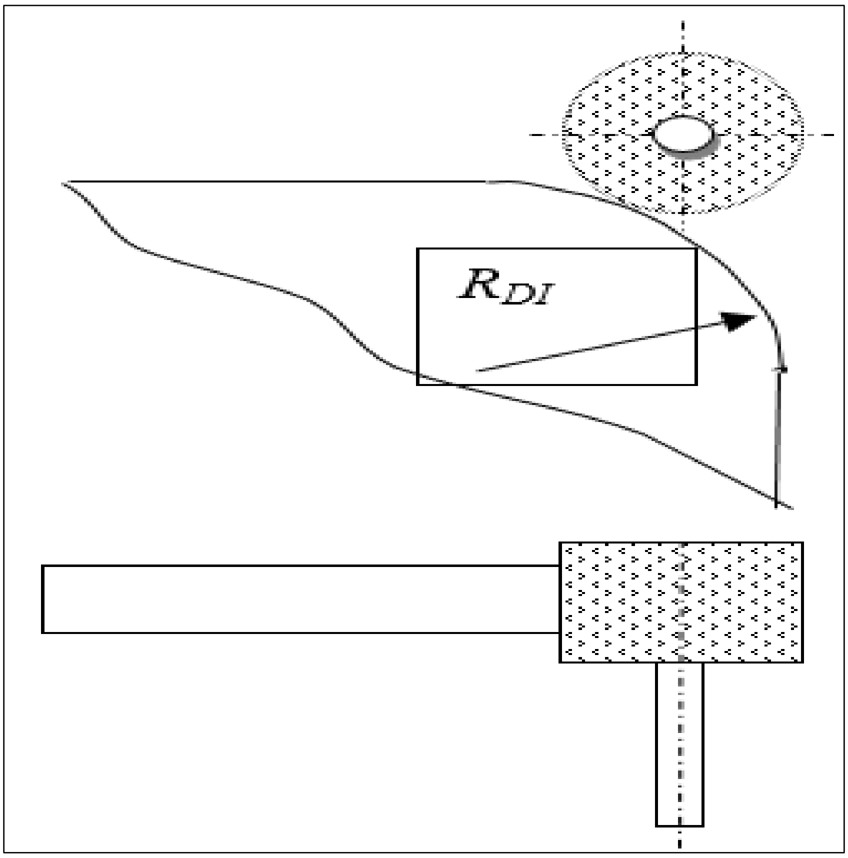

Figure 11: Scheme for processing a surface rounded along the outer radius using an elastic polymer-abrasive wheel.
Source: Authors, (2025).

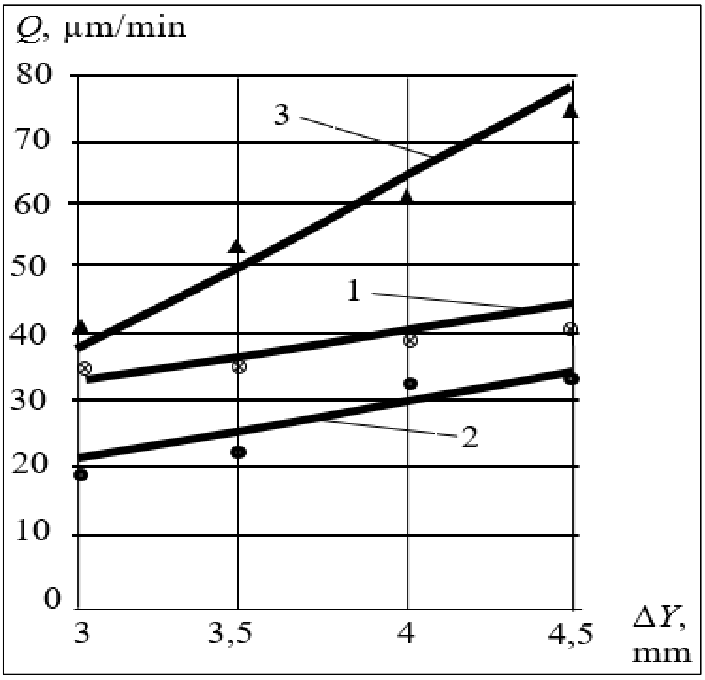

Figure 12: Dependence of the process productivity Q on deformation ΔY (V=606.3 m/min, F_R =130 mm/min) for the CF-FB-0.5 AFIN wheel.
Source: Authors, (2025).

1 – processing of a flat surface;
2 – processing of a surface rounded along the outer radius R_{de}=120 mm;
3 – processing of a surface rounded along the inner radius R_{DI}=120 mm.

As an example, Figures 12 and 13 show the dependences of the process productivity indicator Q on the tool deformation ΔY and the cutting speed V for one of the tools studied. In Figures 12 and 13, dots represent experimental data, while lines represent theoretically calculated data.

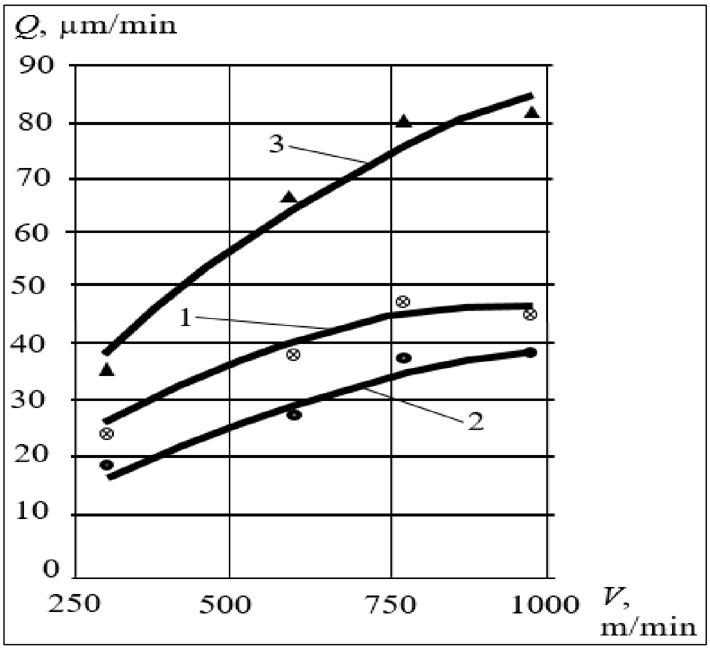

Figure 13: Dependence of the process productivity Q on the cutting speed V (ΔY= mm, F_R =130 mm/min)
for the CF-FB-0.5 AFIN wheel.
Source: Authors, (2025).

1 – processing of a flat surface;
2 – processing of a surface rounded along the outer radius R_{de}=120 mm;
3 – processing of a surface rounded along the inner radius R_{DI}=120 mm.

IV. CONCLUSIONS

The flexible polymer-abrasive wheels investigated in this study can be effectively used for processing surfaces of parts made from aluminum alloys used in aerospace engineering. The research has revealed that the geometric features of the processed surfaces have a significant impact on the efficiency of the machining process. For instance, when processing a surface rounded along the outer radius R_{de}=120 mm, the process productivity decreases by 5...40%, whereas when processing a surface rounded along the inner radius R_{DI} =120 mm, the productivity increases by 10...80% depending on the type of flexible polymer-abrasive wheel and the processing conditions. This effect is explained by substantial changes in the contact area and, consequently, the number of active abrasive grains, as well as the cutting forces involved. These findings must be taken into consideration when designing technological operations for finishing parts with flexible polymer-abrasive tools.

V. REFERENCES

[1] T. Zhanibekov, T. Nikonova, K. I. Imasheva [et al.], “Studying the Processes that Take Place in Vibroabrasive Machining of Complex-Shaped Parts”, Material and Mechanical Engineering Technology, vol. 3, no. 3, pp. 42-49, 2022.

[2] Y. Zhang and Y. Zou, “Study on Corrective Abrasive Finishing for Workpiece Surface by Using Magnetic Abrasive Finishing Processes”, Machines, vol. 10, no. 2, 2022. DOI 10.3390/machines10020098.

[3] X. Zhang, X. Zhao, Bo. Cheng [et al.], “Finishing mechanism modelling on magnetic abrasive finishing behaviours with core-shell magnetic abrasive particles”, The International Journal of Advanced Manufacturing Technology, vol. 129, no. 1-2, pp. 573-585, 2023.

[4] G. Prasad, G. S. Vijay and Kamath C. R., “Evaluation of tool wear and surface roughness in high-speed dry turning of Incoloy 800”, Cogent Engineering, vol. 11, no. 1, 2024. DOI https://doi.org/10.1080/23311916.2024.2376913.

[5] J. C. Puoza “Experimental study on abrasive water-jet polishing of cemented carbide and polycrystalline diamond tools”, International Journal of Abrasive Technology, vol. 9, no. 3, pp. 200-220, 2019.

[6] F. Kara, F. Bayraktar, F. Savaş and O. Özbek “Experimental and statistical investigation of the effect of coating type on surface roughness, cutting temperature, vibration and noise in turning of mold steel”, Journal of Materials and Manufacturing, vol. 2, no. 1, pp. 31-43, 2023. DOI https://doi.org/10.5281/zenodo.8020553.

[7] G. Prasad, G. S. Vijay, R. C. Kamath and H. J. Hemmady “Optimization of the tool wear and surface roughness in the high-speed dry turning of Inconel 800”, Cogent Engineering, vol. 11, no. 1, pp. 1-14, 2024. DOI https://doi.org/10.1080/23311916.2024.2308993.

[8] E. dos Santos Passari, A. J. de Souza and A. M. Vilanova “Surface roughness analysis in finishing end milling of Hardox® 450 steel using multilayer graphene-based nanofluid”, J Braz. Soc. Mech. Sci. Eng., vol. 45, no. 147, 2023. DOI https://doi.org/10.1007/s40430-023-04069-1.

[9] M. R. Policena, C. Devitte, G. Fronza, R. F. Garcia and A. J. Souza “Surface roughness analysis in finishing end-milling of duplex stainless steel UNS S32205”, Int J Adv Manuf Tech., vol. 98, pp. 1617–1625, 2018. DOI https://doi.org/10.1007/s00170-018-2356-4.

[10] M. Moayyedian, A. Mohajer, M. G. Kazemian, A. Mamedov and J. F. Derakhshandeh “Surface roughness analysis in milling machining using design of experiment”, SN Appl Sci., vol. 2:1698, 2020. DOI https://doi.org/10.1007/s42452-020-03485-5.

[11] A. Patil, R. Rudrapati and N. S. Poonawala "Examination and prediction of process parameters for Surface roughness and MRR in VMC-five axis machining of D3 steel by using RSM and MTLBO", Mat Today Proc., vol. 44, no. 1, pp. 2748-2753, 2021. DOI https://doi.org/10.1016/j.matpr.2020.12.700.

[12] R. Hamano, H. R.Costa and T. Chuvas. "Evaluation of machining forces and surface integrity on AISI 304 steel top milling process under different cutting conditions", ITEGAM-JETIA, vol. 05, no. 20, pp. 166-171, 2019. DOI: https://dx.doi.org/10.5935/2447-0228.20190103.

[13] Passari, Émerson, H. Amorim and A. Souza. "Multi-objective optimization of cutting parameters for finishing end milling Hardox® 450", ITEGAM-JETIA, vol. 08, no. 34, pp. 20-28, 2022. DOI: https://doi.org/10.5935/jetia.v8i34.805.

[14] A. V. Ivanova, A. S. Belomestnykh, E. Yu. Semenov and B. B. Ponomarev. "Manufacturing capability of the robotic complex machining edge details", International Journal of Engineering and Technology, vol. 7, no. 5, pp. 1774-1780, 2015.

[15] E. N. Semyonov, A. V. Sidorova, A. E. Pashkov and A. S. Belomestnykh. "Accuracy assessment of Kuka KR210 R2700 Extra Industrial robot", International Journal of Engineering and Technology, vol. 16, no. 1, pp. 19-25, 2016.

[16] K. C. G. Candioto, K. C. Silva, B. S. Linke. "Metal finishing using manual grinding with lamellar sanding wheels as grinding tools", International Journal of Abrasive Technology, vol. 11, no. 2, pp. 119-135, 2022.
DOI: 10.1504/IJAT.2022.128047

[17] Yu. V. Dimov and A. V. Shmatkova. "Interaction of Lobed Wheel with Machined Surface", Russian Engineering Research, no. 7, pp. 707-711, 2011.

[18] Yu. V. Dimov and D. B. Podashev. "Method for determining the parameters of the cutting micro relief of an elastic abrasive tool", Patent RF, no. 2561342, 2015.

[19] Yu. V. Dimov and D. B. Podashev. "Machining forces exerted by an Elastic Abrasive Wheel", Russian Engineering Research, vol. 38, no. 12, pp. 932-937, 2018.

[20] Yu. V. Dimov and D. B. Podashev. "Experimental research of cutting forces at finishing processing of machine components by elastic polymer-abrasive circles", IOP: Conferences Series: Materials Science and Engineering, vol. 632, article number 012091, 2019.